Stability Analysis of Boundary and Hybrid Controllers for Indirect Energy Transfer Converters

Or Kirshenboim, *Student Member, IEEE*, and Mor Mordechai Peretz, *Member, IEEE*

***Abstract*—In boost converters and other indirect energy transfer topologies, transient-oriented controllers are designed to facilitate a dynamic response that may range from minimum time up to minimum output voltage deviation. Since analytical definitions for these control laws can become quite complex, a large-signal stability verification is not immediate. This paper explores the existence of stability of indirect energy transfer converters that are controlled by either boundary or hybrid controllers and introduces a new simplified procedure for examination of large-signal stability of a given converter and load type using a graphical–analytical approach. The stability analysis and examination method are demonstrated on a boost converter loaded by resistive load and constant current load. The stability conditions are verified using a 30 W 3.3-to-12 V boost converter prototype, controlled by a programmable-deviation controller and time-optimal controller, verifying their large-signal stability.**

***Index Terms*—Boundary control, digital control, stability analysis, state space.**

I. Introduction

In recent years, there has been a sharp increase in interest for more compact, lighter, energy-efficient, and economical power sources. Tighter output voltage regulation, faster response time to load changes and lower volume are of major concern in the design of present-day switch-mode power supplies (SMPSs). To obtain fast transient response, several transient-oriented controllers, e.g., time-optimal controllers (TOCs) have been introduced [1]–[8]. These controllers integrate nonlinear, state-variable-based control laws, which allow convergence limited by the slew rate of the reactive components. To further improve the system performance and reduce the total volume of the converter, in particular for boost-type converters, reduction of the components' stress has been assigned as the primary performance goal [9]. This is achieved by defining the output voltage deviation as a control objective rather than the convergence time [10], [11].

Transient-oriented controllers can be generally divided into two types, boundary or hybrid. Boundary controllers [12]–[18], among them hysteretic and sliding-mode controllers, are geometry-based methods that split the state-plane such that in one side of the boundary the operation is governed by the on state and by the off state at the other side of the boundary. Hybrid controllers [1]–[8], [10], [11], [19]–[25] switch between two or more control laws based on the system state variables in order to obtain the performance goals. Within the context of switch-mode applications, the hybrid control law typically incorporates a steady-state linear controller (i.e., PI or PID), to allow constant operating frequency, which simplifies the design of the power converter.

Following the proliferation of digital control technology [26]–[31], both boundary and hybrid control methods have regained popularity. In particular, sliding-mode control [32]–[35] and its extension have been exemplified for buck converters [36]–[39]. As frequently reported in many cases, realization of these controllers requires extensive computation resources as well as precise information on the system parameters to assure the desired performance and stability of the system. These would prohibit penetration of the controllers into real-world applications.

To overcome the challenges, hardware-efficient control methods with reduced sensitivity to variations of parameters for buck and boost converters have been recently presented in [1], [10] and [11], [15], respectively. There, a hybrid controller combines a boundary-type control for large-signal transient events with a linear steady-state control law. The computing effort and parameter sensitivity can be reduced significantly by the realization of the boundary control law by comparators with reference assignment based on the system behavior during a transient event which is obtained from its state-space representation. The main limitation for the majority of these controllers is that their stability cannot be directly guaranteed using the known techniques since an analytical formulation of the control law is not immediate.

Stability investigations of boundary control and its derivatives, or large-signal stability, for switch-mode converters have been widely studied in the literature by observation and analysis of the state trajectories, either on the state-space [9], [40]–[42] or on the state-energy plane [43] with a primary control objective to obtain fast transient response. Since typical trajectories of switch-mode converters include spirals and hyperboles, it is quite difficult to formulate a control law for both well-defined behavior, simple implementation and that its stability can be assured by simple derivations. An example where existence of stability has been described and analyzed can be found in [1] for the specific case of direct energy transfer buck converter controlled by a hybrid-type, sliding-mode TOC. In cases where the control objective is beyond the simplistic case of fast response such as lower voltage deviation or other constraints added, and in particular indirect energy transfer converters, the pursuit after stability existence criteria to date, is still ongoing.

The objective of this study is to explore the stability criteria of boundary and hybrid control methods for indirect energy transfer converters, delineate the necessary and sufficient conditions for large-signal stability, and to present a graphical-analytical approach to examine the large-signal stability of an arbitrarily given control law that is described on the state-plane. It is

Manuscript received February 16, 2015; revised May 13, 2015; accepted June 26, 2015. Date of publication July 7, 2015; date of current version November 30, 2015. Recommended for publication by Associate Editor G. Escobar.

The authors are with the Center for Power Electronics and Mixed-Signal IC Department of Electrical and Computer Engineering, Ben-Gurion University of the Negev, Beer-Sheva 8410501, Israel (e-mail: orkir@post.bgu.ac.il; morp@ee.bgu.ac.il).

Color versions of one or more of the figures in this paper are available online at http://ieeexplore.ieee.org.

Digital Object Identifier 10.1109/TPEL.2015.2453631

a further objective of this study to examine the behavior and the stability of the programmable-deviation controller for boost converters in [10] which includes the TOC as a particular case. It should be noted that in this paper, the analysis is not limited by the realization method of the controller (whether analog, digital, or mixed-mode) as long as its operation can be described on the state-space.

The rest of the paper is organized as follows: Section II reviews the properties of boundary and hybrid control and discusses the properties of the load-line dependence on the load's type. Section III reviews the recently presented programmable-deviation controller and showing its properties as a boundary controller. A stability analysis of boost converter loaded by resistive load and constant current load is presented in Section IV, including a physical interpretation and a procedure to examine large-signal stability of a given converter. Section IV further extends a generalization of the stability analysis for unknown load type and other indirect energy transfer converters topologies. Experimental results and conclusion are then provided in Sections V and VI, respectively.

II. Review: Boundary Control, Hybrid Control, and the Load-Line

A. Boundary Control

Boundary control is a geometric-based control, which defines a curve of the form $\sigma = f(v_C, i_L) = 0$ on the state-plane called (switching) boundary. It is a generalization of well-known hysteretic-type control methods such as voltage-mode hysteretic control and sliding-mode control. For converters with two possible switching states, a boundary defines when the converter is in on state and when it is in off state. Whenever the converter's states are located on one side of the boundary, e.g., $\sigma > 0$, the operation is governed by an on state, and whenever the states are located on the other side, e.g., $\sigma < 0$, the operation is governed by an off state. Switching between the two states is made when the state trajectory crosses the boundary; thus, a boundary must pass through the desired steady-state operating point $(V_{\rm ref}, I_{\rm ref})$ in order to be able to drive the converter to this point.

The state-plane of a switch-mode converter can be separated to the three different regions, i.e., reflective, refractive, and rejective, according to the properties of every point and the on- and off-state trajectories passing through it [14]. The lines separating these three regions are the load-line (see Section II-C for further details) and the steady-state's on and off trajectories. As a consequence, the operation of a boundary controller can be classified into three modes as well, by the location of the boundary with respect to operation region. Within the context of this study, a boundary controller is defined as *large-signal stable* if it moves the converter's states to the steady-state operating point and keeps it there, resulting in a state error (voltage and current error) approaching zero, limited by the converter switching frequency.

B. Hybrid Control

Hybrid control incorporates two or more control laws. The different control laws can be either different small-signal linear controllers, large-signal nonlinear controllers, or a mixture of both. Switching between these control laws depends on the converter's states, where the objective of switching between the controllers can be either to achieve faster dynamic response, lower voltage, or current overshoots and undershoots, improving efficiency or any other control objective. For example, a hybrid controller such as in [1], can operate as a small-signal linear controller (e.g., PI, PID) when the converter's states are within proximity of the steady-state operating point and as time-optimal-like controller for large-signal compensation when the converter's states are away from the new steady-state operating point, in order to achieve the fastest possible dynamic response.

In a hybrid controller that combines large-signal and small-signal linear controllers, it is not a necessary condition for large-signal stability that the large-signal controller will decrease the state-error toward zero and will maintain it in this point. This is since the small-signal linear controller is in charge of keeping the converter's states at the steady-state operating point, maintaining a zero-state error. The only condition for stability in such a hybrid controller is that the large-signal controller will move the converter's states to the desired steady-state operating point. Thus, a *hybrid controller large-signal stability* exists if the large-signal compensator is capable of bringing the converter's states from any initial condition to the steady-state operating point.

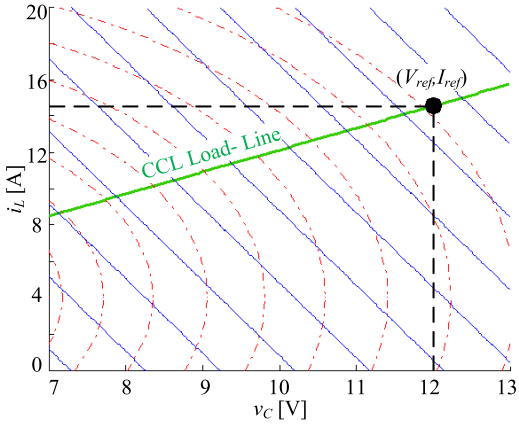

Fig. 1. On and off trajectories and the load-line of a boost converter loaded by a CCL.

C. Load-Line

The load-line of a converter is defined by the set of all its asymptotic points (i.e., possible steady-state operating points) on the state space for $D \in [0,1]$ and for a given load value, where D is the duty ratio of the controlled switch.

Using any of the three methods described in [13] to obtain the load-line of a boost converter loaded by a CCL, it is given by

$$LL_{\rm CCL}(v_C, i_L) = \left\{ v_C, i_L : i_L = \frac{I_o}{V_{\rm in}} v_C \right\} \tag{1}$$

and its state-plane is depicted in Fig. 1. For the CCL case, the on trajectories are straight lines and the off trajectories are ellipses.

In a similar manner for a boost converter loaded by a resistive load (RL), the load-line can be expressed as

$$LL_{\rm RL}(v_C, i_L) = \left\{ v_C, i_L : i_L = \frac{1}{RV_{\rm in}} v_C^2 \right\}. \tag{2}$$

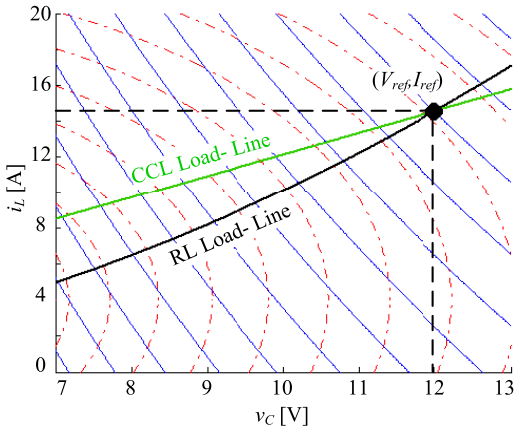

Fig. 2. On and off trajectories and load-line (black) of a boost converter loaded by an RL and the CCL load-line from Fig. 1 (green).

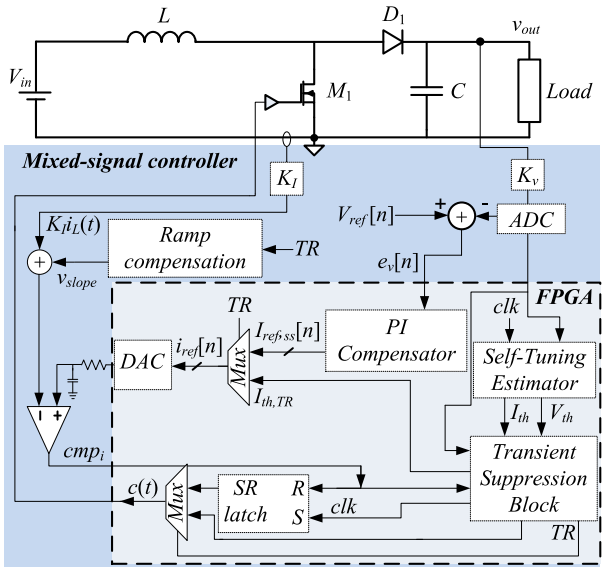

Fig. 3. Programmable-deviation controller regulating operation of a boost converter.

For this case, the on trajectories are exponential and the off trajectories are spirals instead of ellipses. However, within the region of interest for a boost converter where $v_C > V_{\rm in}$ and $i_L > 0$, the off trajectories can be well approximated to an ellipses. The differences between the load-lines of the two cases are depicted in Fig. 2. As can be observed, the load-line of a CCL is higher in i_L than the load-line of an RL, for $v_C < V_{\rm ref}$, which is the relevant region for loading transients.

III. Programmable-Deviation Controller

A programmable-deviation controller has been recently presented in [10]. The controller, schematically presented in Fig. 3, is designed to deal with loading and unloading transients of indirect energy transfer converters. It hybrids a conventional mixed-signal peak current programmed mode (CPM) controller for steady-state voltage regulation and a boundary-type control law for the large-signal transient mode. For the operation of the boundary controller, two additional blocks were added, a

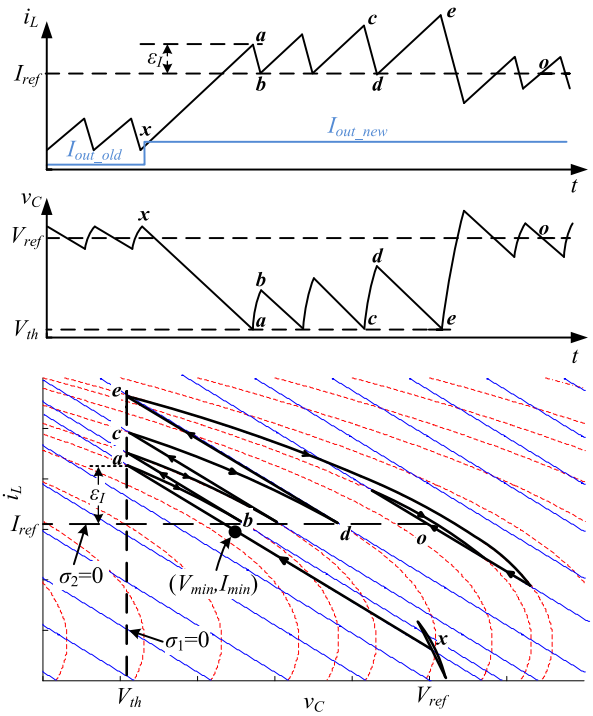

Fig. 4. Operation of the programmable-deviation controller in a boost converter for loading transient (maximum switching frequency is limited). Inductor and load current (top), output voltage (middle), and state-plane representation of the voltage and current (bottom).

transient suppression block and a *self-tuning estimator*. Upon a load transient detection, these blocks take over the task of creating the pulsewidth-modulated signal from the conventional controller and provide transient response with voltage deviation as prescribed by the control objective. The transient suppression block implements a boundary-type control algorithm that dynamically changes the on and off transistor times, based on the information of the load current that is provided by the estimator. Once the transient recovery is completed the controller returns to steady-state operation.

The controller recovers from a loading transient through a two-step process. Upon detection of a transient, during the first step, the transistor of the boost is turned on. Over this period, the controller estimates the new load current and accordingly, sets one switching boundary, i.e., threshold, for the inductor current $I_{\rm th}$ such that it is slightly larger than the new steady-state value $I_{\rm ref}$ (by ε_I), i.e.

$$I_{\rm th} = I_{\rm ref} + \varepsilon_I \tag{3}$$

where the value for ε_I is used to limit the switching frequency.

Once the first current threshold has been reached (point *a*, see Fig. 4), in the second step, the controller measures the output voltage and assigns two switching boundaries as $V_{\rm th} = v_C|_{\text{point } a}$ and $I_{\rm th} = I_{\rm ref}$. From this point and on, the transistor's on time is governed by the voltage boundary and the off time by the current boundary. It should be noted that by assigning the boundaries as prescribed here, the controller operation depends on the quality of the load current estimator alone and is insensitive to any parameter variations or uncertainties. Within the context of this study, the transient action

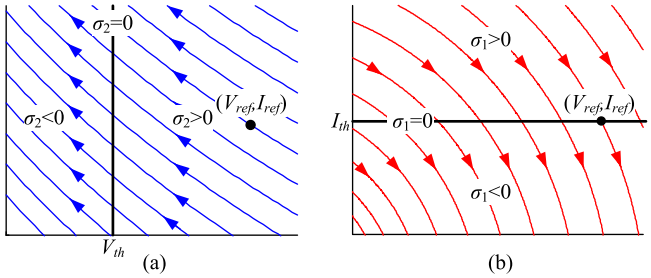

Fig. 5. Programmable-deviation controller switching boundaries for (a) on state (b) off state.

of the programmable-deviation controller can be defined by a boundary-type control where there are switching boundaries σ_1 for the off state ($I_{\rm th}$) and σ_2 for the on state ($V_{\rm th}$), as demonstrated in Fig. 5, and have the expressions of the following form:

$$\sigma_1 = i_L - I_{\rm th}$$
$$\text{where}: \quad \sigma_1 < 0 \rightarrow \text{on}$$
$$\sigma_1 > 0 \rightarrow \text{off} \tag{4}$$
$$\sigma_2 = v_C - V_{\rm th}$$
$$\text{where}: \quad \sigma_2 < 0 \rightarrow \text{off}$$
$$\sigma_2 > 0 \rightarrow \text{on}. \tag{5}$$

As can be observed from Fig. 2, the minimum output voltage deviation [$(V_{\rm min}, I_{\rm min})$, see Fig. 4] is obtained where the first on state trajectory intersects the load-line. However, convergence to the steady-state operating point (point o) from this point would require operation at a very high switching frequency (theoretically infinite for the case when $V_{\rm th}$ is equal to $V_{\rm min}$) and, as such, is not practical. Therefore, the switching frequency range is limited by the additional charging of ε_I as depicted in Fig. 4. Moreover, the programmable-deviation controller can produce a time-optimal response as well, by selecting the specific ε_I to obtain charge balance during a single on-off cycle. This makes the time-optimal control a particular case of the programmable-deviation control, as demonstrated in Fig. 6. In this case, the boundary-type controller can be written as a single boundary expression

$$\sigma_{2,\rm TOC} = v_C - v_C|_{\text{point } a,\rm TOC}$$
$$\text{where}: \quad \sigma_2 < 0 \rightarrow \text{off}$$
$$\sigma_2 > 0 \rightarrow \text{on}. \tag{6}$$

Section IV delineates the region where stability of the programmable-deviation controller exists for the case of loading transients.

IV. Stability Analysis

This section aims to delineate the region on the state-plane where large-signal stability exists. In the context of indirect energy transfer converters, the objective of the transient controllers ranges from minimum convergence time, i.e., time-optimal control, up to minimum output voltage deviation. Therefore, examination of large-signal stability is essential within the control objective range.

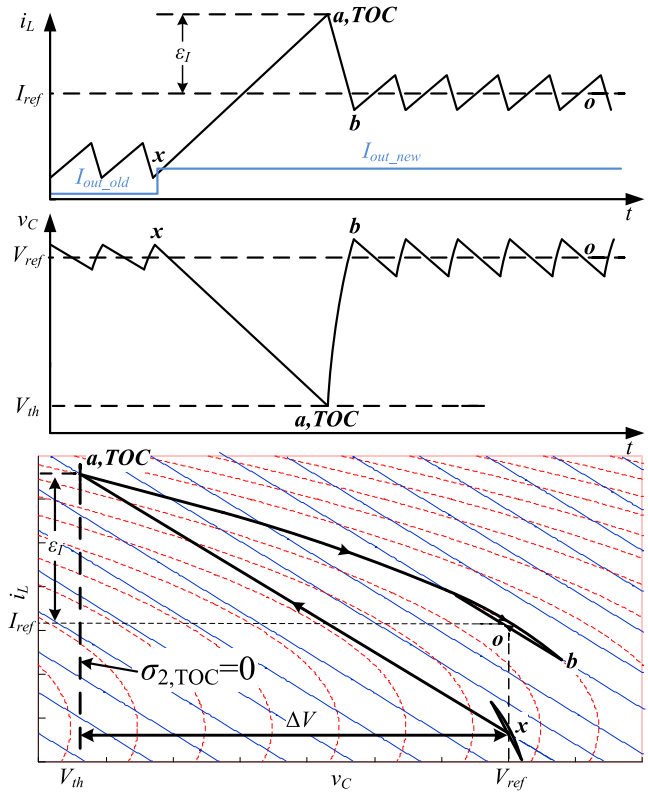

Fig. 6. Time-optimal response of boost converter controlled by a programmable-deviation controller during a loading transient: inductor and load current (top), output voltage (middle), and state-plane representation of the voltage and current (bottom).

Since the analytical definition and derivations for stability of a large-signal controller may become quite complex, the methodology of this study is to first define the limits of the stability region on the state-plane for a given converter and load type. Since the analysis for the stability region is based on the physical properties of the converter alone, then the evaluation per controller can be obtain graphically on any controller that can be drawn on the state-plane. By doing so, the steps of the procedure are similar to any small-signal linear analysis that is in practice today, e.g., Bode, Nyquist, or Nichols.

The limits of the stability region for a given converter are obtained by analysis of a control method that describes a curve (i.e., switching surface) in the state-plane. In particular, the well-known sliding-mode control is adopted because of its well-defined analytical description as well as the stability analysis for switch-mode converters [32]. The shape, or template, of the sliding-mode controller is chosen such that it is related to the physical properties of the converter, i.e., its load-line. This choice assists to conclude the results based on the converter's physical properties, rather than on a specific control method.

The outcome of the analysis leads to a definition of the *large-signal region of convergence* (ROC), where the convergence to zero state error is guaranteed for boundary controllers and passing through the steady-state operating point is guaranteed for hybrid controllers. Based on the analysis, a simplified procedure to examine large-signal stability of any arbitrary controller by a graphical–analytical approach is provided in Section IV-D.

In the following stability analyses, an ideal boost converter is assumed, neglecting the capacitor's ESR, MOSFET's $R_{\mathrm{DS(on)}}$ and diode forward voltage V_{D}. It should be noted that since the stability analysis is carried out under the assumption of small ripple approximation [32], the output voltage ripple has not been taken into account. The effect of the capacitor's ESR on the stability analysis is negligibly small and estimated as the increment or the output voltage ripple. This shifts the stability boundaries on the output voltage axis by the value of the additional voltage ripple due to the ESR. It is also assumed that the delay caused by the load transient detection does not affect the system's response as detailed in [10].

A. Resistive Load Stability Analysis

For a boost converter loaded by an RL, the load-line is a parabola; therefore, a parabolic switching surface σ_{RL} is selected

$$\sigma_{\mathrm{RL}} = i_L - I_{\mathrm{ref}} - \lambda_{\mathrm{RL}}(v_C^2 - V_{\mathrm{ref}}^2). \tag{7}$$

The converter's average model can be expressed as

$$\begin{aligned} \frac{dv_C}{dt} &= -\frac{v_C}{RC} + \frac{i_L}{C}(1-u) \\ \frac{di_L}{dt} &= \frac{V_{\mathrm{in}}}{L} - \frac{v_C}{L}(1-u) \end{aligned} \tag{8}$$

where u is the control input. The equivalent control u_{eq} along the switching surface is derived by taking the derivative of σ_{RL} with respect to time and setting $\dot{\sigma}_{\mathrm{RL}} = 0$ [44] and can be expressed as

$$u_{\mathrm{eq}} = 1 - \bar{u}_{\mathrm{eq}}, \qquad \bar{u}_{\mathrm{eq}} = \frac{V_{\mathrm{in}} - L di_L/dt}{v_C}. \tag{9}$$

Assuming small current ripple, $V_{\mathrm{in}} \gg L di_L/dt$ [32], hence $u_{\mathrm{eq}} = 1 - v_C/V_{\mathrm{in}}$. Substituting u_{eq} into (8) yields

$$i_L = \frac{v_C^2}{RV_{\mathrm{in}}} + \frac{Cv_C}{V_{\mathrm{in}}}\frac{dv_C}{dt}. \tag{10}$$

To examine whether the trajectories along the switching surface lead to a unique steady-state operating point, let $\tilde{v}_C$ and $\tilde{i}_L$ be the current and voltage errors, respectively, defined by the following relationship:

$$\begin{aligned} \tilde{v}_C &= v_C - V_{\mathrm{ref}} \\ \tilde{i}_L &= i_L - I_{\mathrm{ref}}. \end{aligned} \tag{11}$$

Substituting (10) into (11) yields

$$\tilde{i}_L + I_{\mathrm{ref}} = \frac{(\tilde{v}_C + V_{\mathrm{ref}})^2}{RV_{\mathrm{in}}} + \frac{C}{V_{\mathrm{in}}}(\tilde{v}_C + V_{\mathrm{ref}})\frac{d(\tilde{v}_C + V_{\mathrm{ref}})}{dt}. \tag{12}$$

The expression obtained in (12) can be separated into two parts, one that represents the dc component, I_{DC}, and the other that represents the time-dependent ac component i_{AC}

$$i_{\mathrm{DC}} = I_{\mathrm{ref}} = \frac{V_{\mathrm{ref}}^2}{RV_{\mathrm{in}}} \tag{13}$$

$$i_{\mathrm{AC}} = \tilde{i}_L = \frac{\tilde{v}_C^2}{RV_{\mathrm{in}}} + 2\frac{V_{\mathrm{ref}}\tilde{v}_C}{RV_{\mathrm{in}}} + \frac{CV_{\mathrm{ref}}}{V_{\mathrm{in}}}\frac{d\tilde{v}_C}{dt} + \frac{C}{2V_{\mathrm{in}}}\frac{d(\tilde{v}_C^2)}{dt}. \tag{14}$$

The dc part is, in fact, the desired steady-state operating point. Therefore, if $i_{\mathrm{AC}} \underset{t\to\infty}{\longrightarrow} 0$ along the switching surface, the system is asymptotically stable and converges to the dc steady-state point. By substituting (11) and (14) into the switching surface $\sigma_{\mathrm{RL}} = 0$ defined in (7) and after some manipulations, the following nonlinear differential equation is obtained:

$$\begin{aligned} &\frac{d(\tilde{v}_C^2 + 2V_{\mathrm{ref}}\tilde{v}_C)}{dt} \\ &\quad + \frac{2V_{\mathrm{in}}}{C}\left(\frac{1}{RV_{\mathrm{in}}} - \lambda_{\mathrm{RL}}\right)(\tilde{v}_C^2 + 2V_{\mathrm{ref}}\tilde{v}_C) = 0. \end{aligned} \tag{15}$$

A variable replacement of $x = \tilde{v}_C^2 + 2V_{\mathrm{ref}}\tilde{v}_C$ results in the following first-order linear differential equation:

$$\frac{dx}{dt} + \frac{2V_{\mathrm{in}}}{C}\left(\frac{1}{RV_{\mathrm{in}}} - \lambda_{\mathrm{RL}}\right)x = 0. \tag{16}$$

Using (16), the stability condition of the switching surface can be obtained. The equation is stable for

$$\lambda_{\mathrm{RL}} < \frac{1}{RV_{\mathrm{in}}} = \lambda_{\mathrm{RL,max}} \tag{17}$$

i.e., $x \underset{t\to\infty}{\longrightarrow} 0 \Leftrightarrow \lambda_{\mathrm{RL}} < \lambda_{\mathrm{RL,max}}$. Therefore, $\tilde{v}_C$ is asymptotically stable and converges toward either one of two equilibria $\tilde{v}_C = 0, \tilde{v}_C = -2V_{\mathrm{ref}}$. Since $\tilde{v}_C = -2V_{\mathrm{ref}}$ means that v_C converges to $-V_{\mathrm{ref}}$, a negative output voltage, this equilibrium is not valid for a boost converter. Since $\tilde{v}_C \underset{t\to\infty}{\longrightarrow} 0$ then $i_{\mathrm{AC}} \underset{t\to\infty}{\longrightarrow} 0$ as well, and the state variables converges to $(V_{\mathrm{ref}}, I_{\mathrm{ref}})$. Hence, by selecting the switching surface (7) that satisfies condition (17), an asymptotical stability is guaranteed.

Sliding-mode control is a particular case of boundary control and requires two more conditions: existence and reachability. The existence condition is related to the reflective region, and sliding-mode operation occurs when the system is operating in reflective mode. Reachability condition is related to the operation in the reflective or refractive regions, but not in the rejective one. Although the switching surface of (7) is always reachable, it needs to be reachable near the steady-state operating point as well, otherwise the system converges to undesirable limit cycles. Thus, another condition to guarantee that the switching surface does not pass in a rejective region is essential, as follows:

$$\begin{aligned} \left.\frac{di_L}{dv_C}\right|_{\substack{\text{'off'} \\ (v_C, i_L) = (V_{\mathrm{ref}}, I_{\mathrm{ref}})}} &= 2\lambda_{\mathrm{RL}}V_{\mathrm{ref}} \\ > -\frac{RCV_{\mathrm{in}}}{LV_{\mathrm{ref}}} = \left.\frac{di_L}{dv_C}\right|_{\substack{\text{'on'} \\ (v_C, i_L) = (V_{\mathrm{ref}}, I_{\mathrm{ref}})}} &, \end{aligned} \tag{18}$$

therefore

$$\lambda_{\mathrm{RL,min}} = -\frac{RCV_{\mathrm{in}}}{2LV_{\mathrm{ref}}^2}. \tag{19}$$

Combining (17) and (19) results in the stability limits for any boost converter loaded by an RL as

$$-\frac{RCV_{\mathrm{in}}}{2LV_{\mathrm{ref}}^2} < \lambda_{\mathrm{RL}} < \frac{1}{RV_{\mathrm{in}}} \tag{20}$$

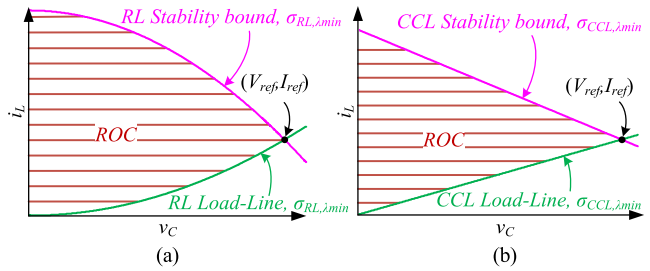

Fig. 7. Illustration of typical ROC for boost converter loaded by a (a) resistive load, (b) constant current load.

which guarantees that for any controller that is defined within these limits, the system will operate either in reflective mode or refractive mode (or both) and will be asymptotically stable. Thus, the ROC for this case can be depicted on the state-plane as in Fig. 7(a), bounded by the curve $\sigma_{\mathrm{RL},\lambda\max}$, which is the load-line and the curve $\sigma_{\mathrm{RL},\lambda\min}$, which is the upper limit, namely, *stability bound*.

B. Constant Current Load Stability Analysis

For a boost converter loaded by a CCL, the load-line is linear and a linear switching surface σ_{CCL} is selected

$$\sigma_{\mathrm{CCL}} = i_L - I_{\mathrm{ref}} - \lambda_{\mathrm{CCL}}\left(v_C - V_{\mathrm{ref}}\right) \tag{21}$$

and the converter's average model can be expressed as

$$\begin{aligned} \frac{dv_C}{dt} &= -\frac{I_o}{C} + \frac{i_L}{C}(1-u) \\ \frac{di_L}{dt} &= \frac{V_{\mathrm{in}}}{L} - \frac{v_C}{L}(1-u). \end{aligned} \tag{22}$$

In a manner similar to the stability analysis in the earlier section for the RL case, the asymptotical stability condition for the CCL case can be expressed as

$$\lambda_{\mathrm{CCL}} < \frac{I_o}{V_{in}} = \lambda_{\mathrm{CCL,max}} \tag{23}$$

which guarantees convergence of the state variables to $(V_{\mathrm{ref}}, I_{\mathrm{ref}})$. In the case of CCL, as opposed to RL, reachability is not guaranteed for every λ_{CCL}; therefore, another condition is necessary to guarantee reachability of the switching surface, obtained from the slope of the on trajectory that passes through the steady-state operating point, that is

$$\lambda_{\mathrm{CCL}} > -\frac{CV_{\mathrm{in}}}{LI_o} = \lambda_{\mathrm{CCL,min}}. \tag{24}$$

Combining (23) and (24) results in the stability limits of

$$-\frac{CV_{\mathrm{in}}}{LI_o} < \lambda_{\mathrm{CCL}} < \frac{I_o}{V_{\mathrm{in}}}. \tag{25}$$

The ROC for this case is depicted in Fig. 7(b). As demonstrated in Fig. 2, the load-line of the CCL case is higher (in i_L) than the load-line of the RL case; therefore, it can be concluded that the lower bound of the ROC (e.g., its load-line) for the CCL case is stricter than the lower bound of the RL case in case of a loading transient.

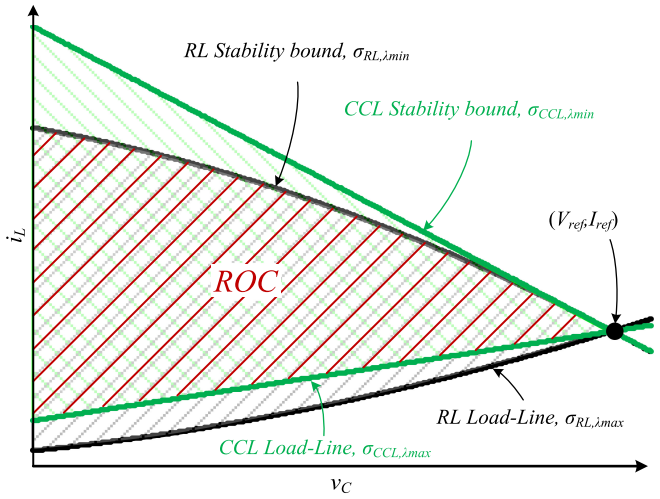

Fig. 8. ROC for a boost converter loaded by an unknown load type. Green—CCL stability boundaries, black—RL stability boundaries.

In the case where the load type is unknown, the ROC can be determined by merging the stability regions of the RL and CCL cases. When analyzing the two ROCs for the same converter parameters (input voltage, output power, inductor, and capacitor), it appears that there is a region on the state-plane that is common for both ROCs (the intersection of the two ROCs), as depicted in Fig. 8. The boundaries of this intersection region are $\sigma_{\mathrm{RL},\lambda\min}$ and $\sigma_{\mathrm{CCL},\lambda\max}$ that are expressed with a relationship to the output power of the converter (P_{out}) and is given by

$$\begin{aligned} \sigma_{\mathrm{RL},\lambda\min} &= i_L - I_{\mathrm{ref}} - \frac{CV_{\mathrm{in}}}{2LP_{\mathrm{out}}}\left(V_{\mathrm{ref}}^2 - v_C^2\right) \\ \sigma_{\mathrm{CCL},\lambda\max} &= i_L - I_{\mathrm{ref}} + \frac{P_{\mathrm{out}}}{V_{\mathrm{in}}V_{\mathrm{ref}}}\left(V_{\mathrm{ref}} - v_C\right). \end{aligned} \tag{26}$$

Therefore, the ROC for an unknown type of load can be expressed as

$$\begin{aligned} \mathrm{ROC} = \Big\{ & v_C, i_L : I_{\mathrm{ref}} + \tfrac{P_{\mathrm{out}}}{V_{\mathrm{in}}V_{\mathrm{ref}}}\left(v_C - V_{\mathrm{ref}}\right) < i_L < I_{\mathrm{ref}} \\ & - \frac{CV_{\mathrm{in}}}{2LP_{\mathrm{out}}}\left(v_C^2 - V_{\mathrm{ref}}^2\right) \Big\}. \end{aligned} \tag{27}$$

C. Physical Interpretation of the Stability Conditions

From conditions (17) and (23) for boost converter loaded by an RL and CCL, respectively, it can be deduced that in order to ensure stability, the switching surface must be above (in i_L) the load-line, for both cases. This observation can also be reinforced by a physical investigation of the converter.

The controller of the converter is in charge of bringing the state variables from an initial steady-state operating point to a new one. Each steady-state point indicates an instantaneous energy stored in the reactive components of the converter, i.e., $E = Cv_C^2/2 + Li_L^2/2$. For a new loading event, the stored energy $E_{\mathrm{old}} = CV_{\mathrm{ref}}^2/2 + LI_{\mathrm{old}}^2/2$ must rise up to a new, higher energy $E_{\mathrm{ref}} = CV_{\mathrm{ref}}^2/2 + LI_{\mathrm{ref}}^2/2$. To increase the stored energy over time, the input power P_{in} of the converter must be higher than its output power P_{out}.

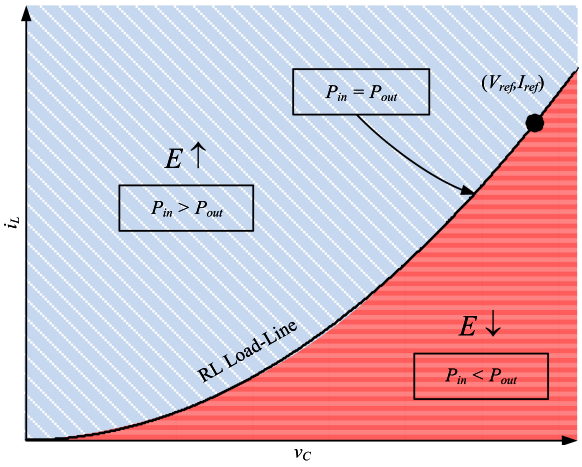

Fig. 9. Input and output power on the boost converter loaded by an RL state-plane.

According to [12] and [33], the load-line represents the states where $P_{\rm in} = P_{\rm out}$ and separates the state-plane to three regions: $P_{\rm in} > P_{\rm out}$, $P_{\rm in} < P_{\rm out}$, and $P_{\rm in} = P_{\rm out}$, as demonstrated in Fig. 9. This means that in order to increase the stored energy from $E_{\rm old}$ to the new steady-state energy $E_{\rm new}$, the state variables must be located at the region where $P_{\rm in} > P_{\rm out}$, i.e., above the load-line (in i_L), which is in agreement with and guaranteed by satisfying conditions (17) and (23) for switching surfaces (7) and (21) of RL and CCL cases, respectively.

The implication of the earlier statement is that any control method that will move the state variables toward the region on the state-plane where $P_{\rm in} > P_{\rm out}$ and will keep them in this region will be able to converge toward the desired steady-state point. It should be noted that this intuitive observation assumes, without loss of generality, an idealized converter that does take into account losses for power balance. This, however, does not affect the results, or strength of the analysis, since the derivations were obtained from a control theory perspective rather than power balance.

D. Stability Examination Procedure

Using the earlier analysis and observations, a generalized method to examine the large-signal stability for a given converter and load type is provided. The procedure is as follows:

1) derive and draw the converter's on and off state trajectories on the state-plane;
2) on the same plot, draw the load-line per the specific load type, or assume constant current load for more strict requirements;
3) using the same plot, draw the stability bound per the load type;
4) given output power level and in case that the load type is unknown, (27) can be used to obtain the ROC;
5) draw the controller curve or switching surface per the control objective;
6) verify that the controller maintains the converter's states within the ROC, i.e., the load-line and the stability bound. If so, the system is asymptotically stable, otherwise, it is unstable.

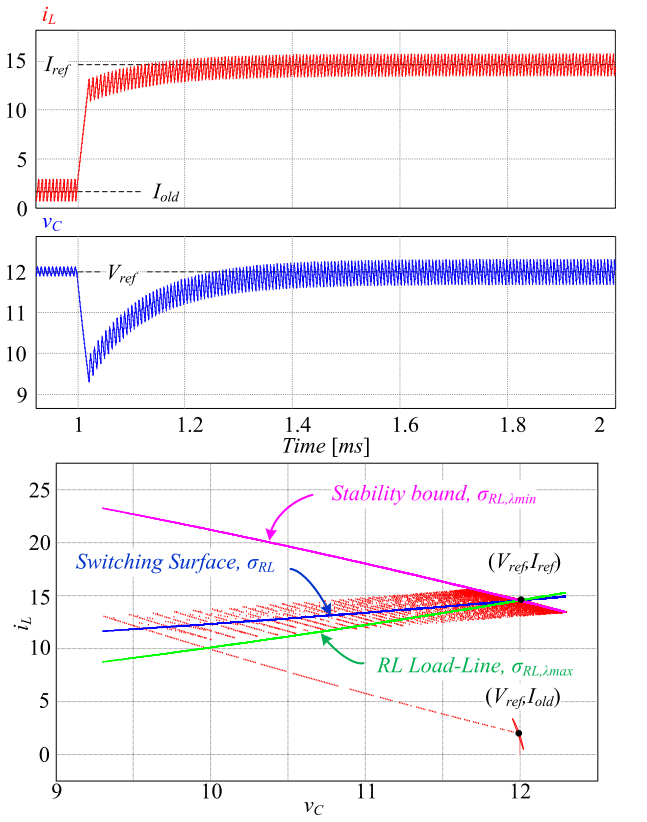

Fig. 10. Simulated boost converter loaded by an RL loading transient from $I_{\rm out,old} = 0.55$ A to $I_{\rm out,new} = 4$ A, $\lambda_{\rm RL} = 0.5\,\lambda_{{\rm RL},max} < \lambda_{\rm RL,max}$, switching surface is above the load-line (bottom—green) and under the stability bound (bottom—magenta), i.e., within the ROC, and the state variables converge to the new steady-state operating point ($V_{\rm ref}, I_{\rm ref}$). Inductor current (top—red), output voltage (middle—blue), and state-plane representation of the voltage and current (bottom). System parameters: $V_{\rm in} = 3.3$ V, $V_{\rm out} = 12$ V, $I_{\rm old} = 2$ A, $I_{\rm ref} = 14.5$ A, $L = 6.8$ μH, and $C = 30$ μF.

Following the earlier procedure, rigorous theoretical analysis per case of a system-controller setting is no longer required. That is, mathematically describing and solving for the large-signal stability can be avoided and replaced by the graphical–analytical method of this study.

To demonstrate the stability examination procedure and verify its validity, a simulation test bench has been created. The results presented in Figs. 10 through 13 have been carried out on a boost converter loaded by RL and controlled by a boundary and programmable-deviation controllers for loading transient. Fig. 10 shows a stable operation of boundary controller with switching surface within the ROC and indeed the system converges toward the new steady-state operating point. Fig. 11 depicts the operation of a boundary controller with switching surface outside the ROC, lower than the load-line, and the system diverges and cannot reach the new steady-state operating point. Fig. 12 presents the programmable-deviation controller operation. As can be observed, the controller maintains the state variables within the ROC and the system passes through the steady-state operating point, where the steady-state linear controller operation takes over. Fig. 13 shows the programmable-deviation controller when operating as a time-optimal controller. The stability of the controller is verified by following the earlier

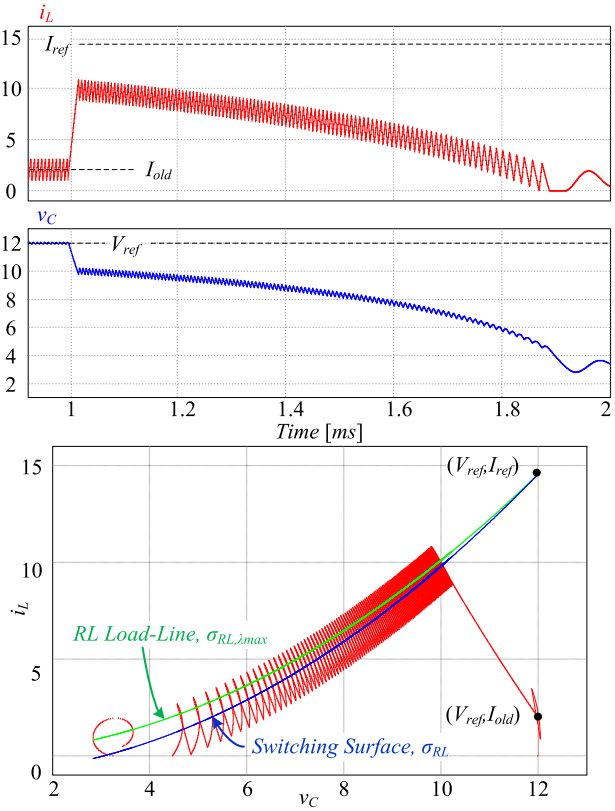

Fig. 11. Simulated boost converter loaded by an RL loading transient from $I_{\mathrm{out,old}} = 0.55$ A to $I_{\mathrm{out,new}} = 4$ A, $\lambda_{\mathrm{RL}} = 1.07\lambda_{\mathrm{RL,max}} > \lambda_{\mathrm{RL,max}}$, switching surface (bottom—blue) is slightly lower than the load-line (bottom—green), i.e., outside the ROC, and the state variables diverge from the new steady-state operating point $(V_{\mathrm{ref}}, I_{\mathrm{ref}})$. Inductor current (top—red), output voltage (middle—blue), and state-plane representation of the voltage and current (bottom). System parameters: $V_{\mathrm{in}} = 3.3$ V, $V_{\mathrm{out}} = 12$ V, $I_{\mathrm{old}} = 2$ A, $I_{\mathrm{ref}} = 14.5$ A, $L = 6.8$ μH, and $C = 30$ μF.

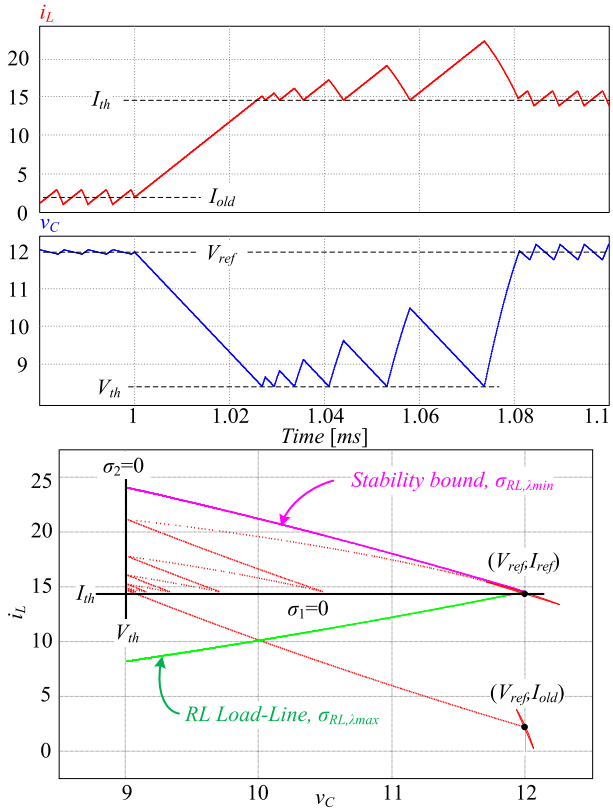

Fig. 12. Simulation of a loading transient of boost converter loaded by an RL using programmable-deviation control. The controller keeps the state variables above the load-line (bottom—green) and under the stability bound (bottom—magenta), i.e., within the ROC, and they converge to the new steady-state operating point $(V_{\mathrm{ref}}, I_{\mathrm{ref}})$. Inductor current (top—red), output voltage (middle—blue), and state-plane representation of the voltage and current (bottom). System parameters: $V_{\mathrm{in}} = 3.3$ V, $V_{\mathrm{out}} = 12$ V, $I_{\mathrm{old}} = 2$ A, $I_{\mathrm{ref}} = 14.5$ A, $L = 6.8$ μH, and $C = 30$ μF.

procedure and setting the controller in this case as described in (6). It can be seen that the controller maintains the state variables within the ROC and the system is asymptotically stable.

The relationship between the controller location on the state-plane (with respect to its geometrical distance from the load-line and the stability bound) and the resultant time response is qualitatively characterized in Fig. 14. For few demonstrative illustrations, the time response resembles the behavior of a second order system with RHP zero. As can be observed, proximity to the load-line results in overdamped response whereas approaching the stability bound, a higher Q underdamped behavior is observed. Setting the controller outside the ROC results in either low Q-like divergence below the load-line [see Fig. 14(a)] or oscillatory divergence above the stability bound [see Fig. 14(e)].

E. Expansion of the Stability Analysis to Other Second-Order Indirect Energy Transfer Converters

By inspection of the state-plane for indirect energy transfer converters with two reactive components, high resemblance is found in their on and off state trajectories to a boost converter. For example, in the case of a noninverting buck–boost (NIBB) converter, the on-state trajectories are exactly matched with the ones in a boost converter and the off-state trajectories of the NIBB converter are shifted left by a constant value of V_{in} (for the same converter's parameters: L, C, V_{in}, V_o, and P_{out}). Using this insight, the stability analysis of Section IV-A and IV-B can be expanded to other converters as well, by applying a simple transformation of the system's parameters and the state variables (v_C, i_L), with respect to the input voltage V_{in} and the load status (I_o for a CCL case and R for an RL case). The core concept is to transform $(v_C, i_L, V_{in}, I_o, R)$ (as defined in Fig. 15) into $(v_C', i_L', V_{in}', I_o', R')$ and then analyze the converter as if it is a boost converter with the provided stability analysis.

The transformation is detailed here for the NIBB converter, and the transformations for other indirect energy transfer converters are given in Table I.

The state equations of NIBB converter loaded by an RL are

$$\begin{aligned} on: \quad & \frac{dv_C}{dt} = -\frac{v_C}{RC}, \qquad \frac{di_L}{dt} = \frac{V_{\mathrm{in}}}{L} \\ off: \quad & \frac{dv_C}{dt} = \frac{Ri_L - v_C}{RC}, \qquad \frac{di_L}{dt} = -\frac{v_C}{L}, \end{aligned} \tag{28}$$

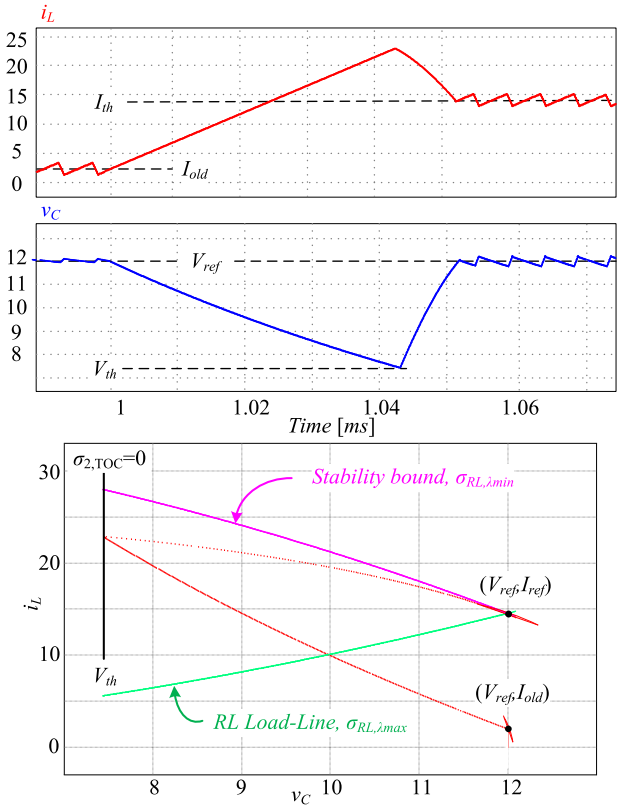

Fig. 13. Simulation of a loading transient of boost converter loaded by an RL using programmable-deviation operating as time-optimal controller. The controller keeps the state variables above the load-line (bottom—green) and under the stability bound (bottom—magenta), i.e., within the ROC, and they converge to the new steady-state operating point ($V_{\rm ref}, I_{\rm ref}$). Inductor current (top—red), output voltage (middle—blue), and state-plane representation of the voltage and current (bottom). System parameters: $V_{\rm in} = 3.3$ V, $V_{\rm out} = 12$ V, $I_{\rm old} = 2$ A, $I_{\rm ref} = 14.5$ A, $L = 6.8$ μH, and $C = 30$ μF.

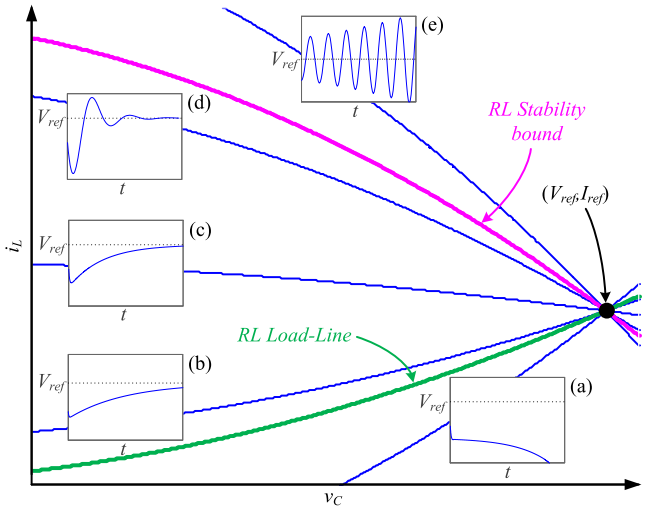

Fig. 14. Illustration of the time response dependency on the geometric location of the controller on the state-plane.

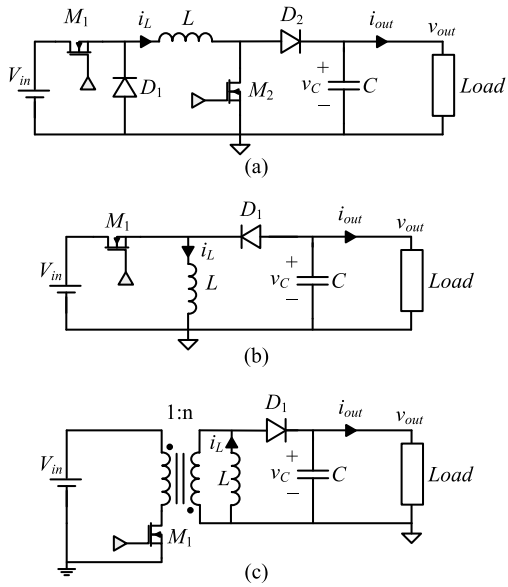

Fig. 15. Second-order indirect energy transfer converters: (a) noninverting buck–boost converter. (b) Buck–boost converter. (c) Flyback converter.

TABLE I
TRANSFORMATIONS OF THE SYSTEM'S PARAMETERS OF SECOND-ORDER INDIRECT ENERGY TRANSFER CONVERTERS

	Constant Current Load	Resistive Load
Noninverting buck–boost	$v'_C = v_C + V_{in}$ $i'_L = i_L$ $V'_{in} = V_{in}$ $I'_o = I_o$	$v'_C = v_C + V_{in}$ $i'_L = i_L$ $V'_{in} = V_{in}$ $R' = \frac{v'_C}{v'_C - V_{in}} R$
Buck–boost	$v'_C = V_{in} - v_C$ $i'_L = i_L$ $V'_{in} = V_{in}$ $I'_o = I_o$	$v'_C = V_{in} - v_C$ $i'_L = i_L$ $V'_{in} = V_{in}$ $R' = \frac{v'_C}{v'_C - V_{in}} R$
Flyback	$v'_C = v_C + nV_{in}$ $i'_L = i_L$ $V'_{in} = nV_{in}$ $I'_o = I_o$	$v'_C = v_C + nV_{in}$ $i'_L = i_L$ $V'_{in} = nV_{in}$ $R' = \frac{v'_C}{v'_C - nV_{in}} R$

and the required transformation is as follows:

$$v'_C = v_C + V_{in}, \qquad i'_L = i_L, \qquad V'_{in} = V_{in},$$
$$R' = \frac{v'_C}{v'_C - V_{in}} R. \tag{29}$$

Substituting (29) into (28) yields the state equations of a boost converter loaded by an RL as depicted in Fig. 16

$$on: \frac{dv'_C}{dt} = -\frac{v'_C}{RC}, \qquad \frac{di'_L}{dt} = \frac{V'_{in}}{L}$$
$$off: \frac{dv'_C}{dt} = \frac{Ri'_L - v'_C}{RC}, \qquad \frac{di'_L}{dt} = \frac{V'_{in} - v'_C}{L}. \tag{30}$$

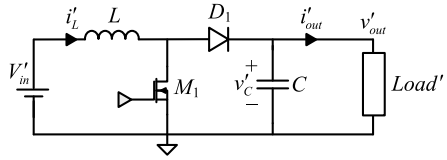

Fig. 16. Boost converter represented with transformed parameters and state variables of other indirect energy transfer converters.

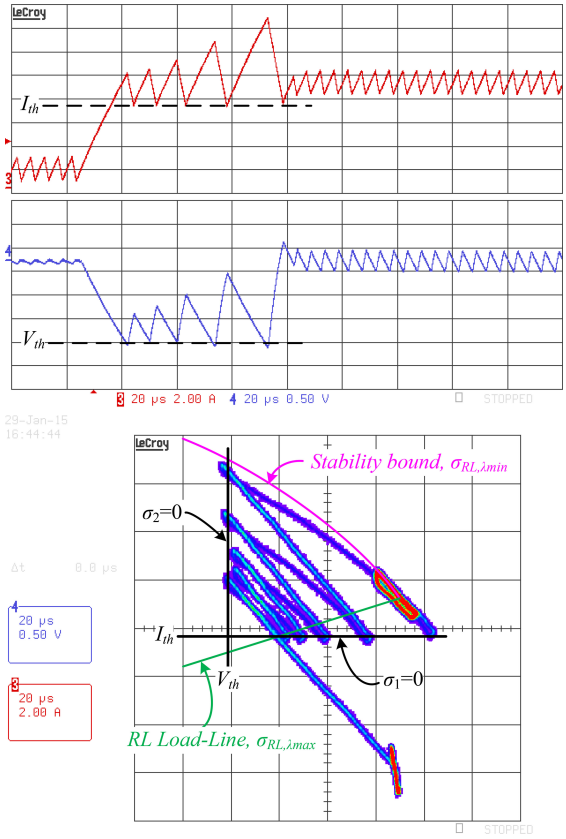

Fig. 17. System's response to a 0.5–2.4 A loading transient using a programmable-deviation controller with boundaries maintaining the converter's states within the ROC. Time scale 20 μs/div. Inductor current (top—red) 2 A/div, output voltage (middle—blue) 0.5 V/div ac coupled, and state-plane representation of inductor current and output voltage (bottom).

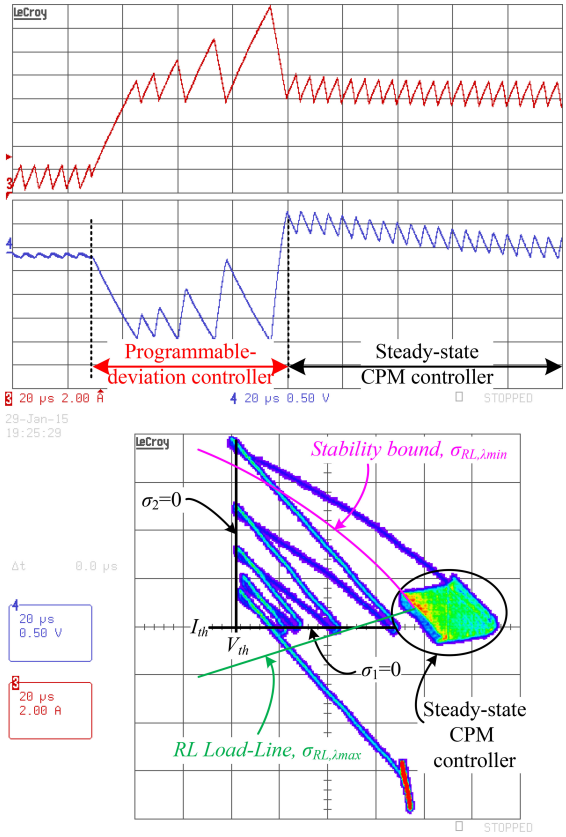

Fig. 18. System's response to a 0.5–2.4 A loading transient using a programmable-deviation controller with boundaries maintaining the converter's states within the stability region, followed by steady-state CPM controller to achieve zero-error state. Time scale 20 μs/div. Inductor current (top—red) 2 A/div, output voltage (middle—blue) 0.5 V/div ac coupled, and state-plane representation of inductor current and output voltage (bottom).

In a similar manner, the transformations required for a CCL case are

$$v'_C = v_C + V_{in}, \qquad i'_L = i_L, \qquad V'_{in} = V_{in}, \qquad I'_o = I_o. \tag{31}$$

As delineated by the derivation concept, the resultant state equations represent a boost converter with the structure as in Fig. 16, from which the analysis has already been established in Section IV-A and IV-B.

V. Experimental Verification

To validate the results of the stability analysis, a 30-W 3.3- to 12-V boost converter prototype was built and tested, using a 6.8 μH inductor and a 30 μF output capacitance and operating at switching frequency of 200 kHz. The converter was loaded by a resistive load type. The prototype is controlled by a hybrid programmable-deviation controller and CPM, implemented on an all-digital FPGA platform [45], including integrated high-performance ADC and DPWM [30].

Fig. 17 shows the system's response to a 0.5–2.4 A loading transient. As can be observed, the programmable-deviation controller keeps the converter's states within the stability region, i.e., above the load-line and below the stability bound, resulting in stable operation and passing through the new steady-state operating point, where the CPM controller takes over and maintains the steady-state operation. Fig. 18 shows the same loading transient response, but in this case the settings for the programmable-deviation controller were set in the same manner with a single difference on the resume conditions of the steady-state controller. This is done to represent operation of the system in the refractive mode, passing through the voltage steady-state value and the small-signal controller (that its stability can be easily guaranteed) is in charge of the bringing the converter's states to the new operating point with zero error.

Fig. 19 shows the system's response to a 0.5–2.4 A loading transient with transient controller settings below the load-line. As can be observed, the controller cannot maintain the converter's states within the stability region, resulting in unstable

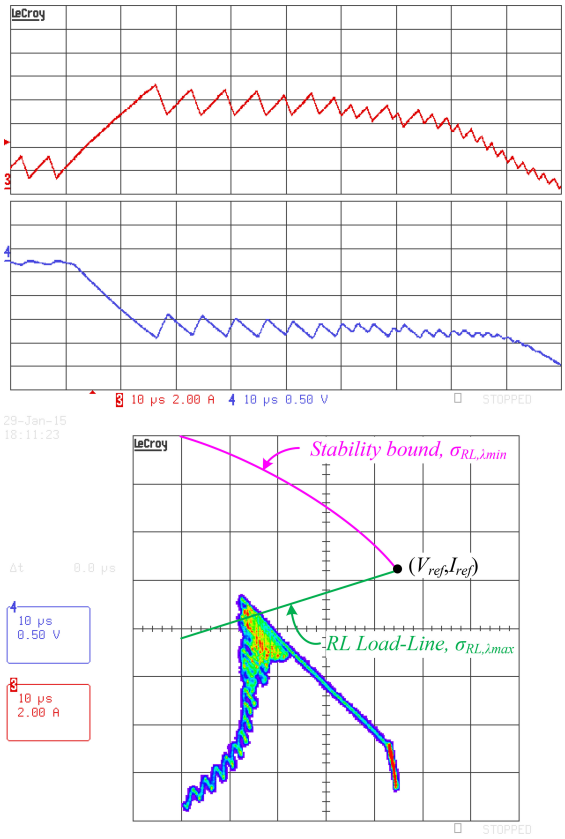

Fig. 19. System's response to a 0.5–2.4 A loading transient using a controller settings below the load-line that cannot maintain the converter's states within the ROC. Time scale 20 μs/div. Inductor current (top—red) 2 A/div, output voltage (middle—blue) 0.5 V/div ac coupled, and state-plane representation of inductor current and output voltage (bottom).

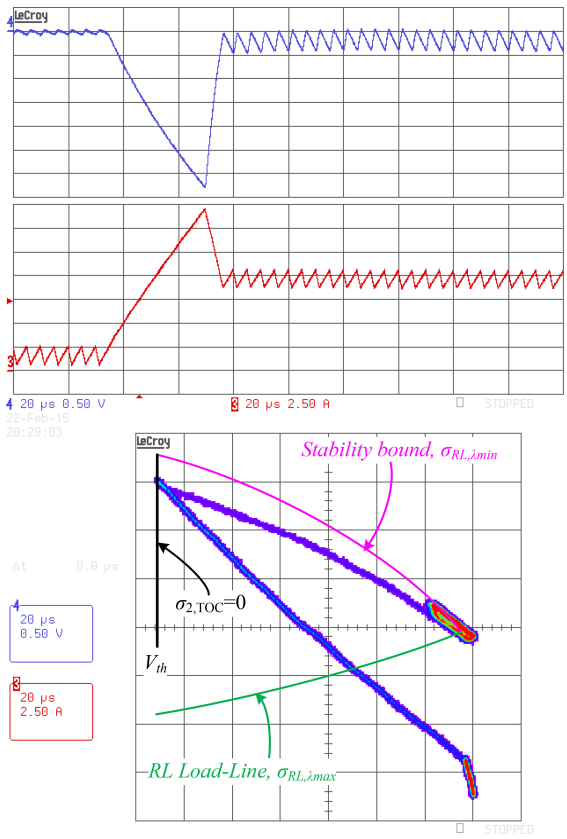

Fig. 20. System's response to a 0.5–2.4 A loading transient using a programmable-deviation controller operating as time-optimal controller with boundary maintaining the converter's states within the ROC. Time scale 20 μs/div. Output voltage (top—blue) 0.5 V/div ac coupled, inductor current (middle—red) 2.5 A/div, and state-plane representation of inductor current and output voltage (bottom).

operation and divergence away from the new steady-state operating point.

A time-optimal response for the same loading conditions is depicted in Fig. 20. The time-optimal controller has been realized as a particular case of the programmable-deviation controller as described by (6). As can be seen, the trajectories are maintained within the ROC in compliance with analysis procedure of Section IV.

VI. Conclusion

A large-signal stability analysis for indirect energy transfer converters has been presented, based on the physical properties of a converter and its load type. A generalized method for examination of large-signal stability of a given converter and load type is provided, delineating the ROC where large-signal stability exists, using a graphical–analytical approach. Once the ROC is extracted, the stability examination method is applicable to any control law that can be described on the state-plane. The conditions for stability, extracted from the stability analysis, were verified on both simulations and experimental test benches, testing the recently presented programmable-deviation controller and verifying the stability of time-optimal controller for a boost converter loaded by a resistive load and a constant current load. The stability analysis and examination method were found to be in excellent agreement with the simulated and experimental results.

References

[1] A. Babazadeh and D. Maksimović, "Hybrid digital adaptive control for fast transient response in synchronous buck DC–DC converters," *IEEE Trans. Power Electron.*, vol. 24, no. 11, pp. 2625–2638, Nov. 2009.

[2] L. Corradini, A. Costabeber, P. Mattavelli, and S. Saggini, "Parameter-independent time-optimal digital control for point-of-load converters," *IEEE Trans. Power Electron.*, vol. 24, no. 10, pp. 2235–2248, Oct. 2009.

[3] A. Babazadeh, L. Corradini, and D. Maksimović, "Near time-optimal transient response in DC–DC buck converters taking into account the inductor current limit," in *Proc. IEEE Energy Convers. Conf. Expo.*, Sep. 2009, pp. 3328–3335.

[4] V. Yousefzedah, A. Babazadeh, B. Ramachandran, E. Alarcon, L. Pao, and D. Maksimović, "Proximate time-optimal control for synchronous buck DC–DC converters," *IEEE Trans. Power Electron.*, vol. 23, no. 4, pp. 2018–2026, Jul. 2008.

[5] L. Corradini, A. Babazadeh, A. Bjeletić, and D. Maksimović, "Current-limited time-optimal response in digitally controlled dc–dc converters," *IEEE Trans. Power Electron.*, vol. 25, no. 11, pp. 2869–2880, Nov. 2010.

[6] G. E. Pitel and P. T. Krein, "Minimum-time transient recovery for DC–DC converters using raster control surfaces," *IEEE Trans. Power Electron.*, vol. 24, no. 12, pp. 2692–2703, Dec. 2009.

[7] E. Meyer, Z. Zhang, and Y.-F. Liu, "An optimal control method for buck converters using a practical capacitor charge balance technique," *IEEE Trans. Power Electron.*, vol. 23, no. 4, pp. 1802–1812, Jul. 2008.

[8] Z. Zhenyu and A. Prodić, "Continuous-time digital controller for high-frequency DC-DC converters," *IEEE Trans. Power Electron.*, vol. 23, no. 2, pp. 564–573, Mar. 2008.

[9] G. E. Pitel and P. T. Krein, "Trajectory paths for dc-dc converters and limits to performance," in *Proc. IEEE Workshop Comput. Power Electron.*, Jul. 2006, pp. 40–47.
[10] M. M. Peretz, B. Mahdavikhah, and A. Prodić, "Hardware-efficient programmable-deviation controller for indirect energy transfer DC–DC converters," *IEEE Trans. Power Electron.*, vol. 30, no. 6, pp. 3376–3388, Jun. 2015.
[11] A. Radić, Z. Lukić, A. Prodić, and R. de Nie, "Minimum deviation digital controller IC for DC-DC switch-mode power supplies," *IEEE Trans. Power Electron*, vol. 28, no. 9, pp. 4281–4298, Sep. 2013.
[12] R. Munzert, "*Boundary control, applied to dc-to-dc converter circuits*," Ph.D. dissertation, ECE Dept. Univ. Illinois, Urbana, IL, USA, Jul. 1995.
[13] R. Munzert and P. T. Krein, "Issues in boundary control," in *Proc. IEEE Power Electron. Spec. Conf.*, Baveno, Italy, Jun. 1996, pp. 810–816.
[14] M. Greuel, R. Muyshondt, and P. T. Krein, "Design approaches to boundary controllers," in *Proc. IEEE Power Electron. Spec. Conf.*, St. Louis, MI, USA, Jun. 1997, pp. 672–678.
[15] J. M. Galvez, M. Ordonez, F. Luchino, and J. E. Quaicoe, "Improvements in boundary control of boost converters using the natural switching surface," *IEEE Trans. Power Electron.*, vol. 26, no. 11, pp. 3367–3376, Nov. 2011.
[16] J. M. Galvez, M. Ordonez, T. T. Nguyen, and F. Luchino, "Boundary control of buck-boost converters: Normalized trajectories and the natural switching surface," in *Proc. IEEE Energy Convers. Conf. Expo*, Sep. 2012, pp. 358–363.
[17] G. G. Oggier, M. Ordonez, J. M. Galvez, and F. Luchino, "Fast transient boundary control and steady-state operation of the dual active bridge converter using the natural switching surface," *IEEE Trans. Power Electron.*, vol. 29, no. 2, pp. 946–957, Feb. 2014.
[18] C. N. Onwuchekwa and A. Kwasinski, "Analysis of boundary control for buck converters with instantaneous constant-power loads," *IEEE Trans. Power Electron.*, vol. 25, no. 8, pp. 2018–2032, Aug. 2010.
[19] P. S. Shenoy, P. T. Krein, and S. Kapat, "Beyond time-optimality: Energy-based control of augmented buck converters for near ideal load transient response," in *Proc. IEEE Appl. Power Electron. Conf. Expo.*, Mar. 2011, pp. 916–922.
[20] D. D. Lu, J. C. Liu, N. K. Poon, and M. H. Pong, "A single phase voltage regulator module (VRM) with stepping inductance for fast transient response," *IEEE Trans. Power Electron.*, vol. 22, no. 2, pp. 417–424, Mar. 2007.
[21] A. Stupar, Z. Lukić, and A. Prodić, "Digitally-controlled steered-inductor buck converter for improving heavy-to-light load transient response," in *Proc. IEEE Power Electron. Spec. Conf.*, Jun. 2008, pp. 3950–3954.
[22] S. Ahsanuzzaman, A. Parayandeh, A. Prodić, and D. Maksimović, "Load-interactive steered-inductor dc-dc converter with minimized output filter capacitance," in *Proc. IEEE Appl. Power Electron. Conf. Expo.*, Feb. 2010, pp. 980–985.
[23] W. Jing, A. Prodic´, and W. T. Ng, "Mixed-signal-controlled flyback-transformer-based buck converter with Improved dynamic performance and transient energy recycling," *IEEE Trans. Power Electron.*, vol. 28, no. 2, pp. 970–984, Feb. 2013.
[24] Y. Wen and O. Trescases, "DC-DC converter with digital adaptive slope control in auxiliary phase to achieve optimal transient response," *IEEE Trans. Power Electron.*, vol. 27, no. 7, pp. 3396–3409, Jul. 2012.
[25] V. Šviković, J. A. Oliver, P. Alou, O. García, and J. A. Cobos, "Synchronous buck converter with output impedance correction circuit," *IEEE Trans. Power Electron.*, vol. 28, no. 7, pp. 3415–3427, Jul. 2013.
[26] M. M. Peretz and S. Ben-Yaakov, "Time-domain design of digital compensators for PWM DC-DC converters," *IEEE Trans. Power Electron.*, vol. 27, no. 1, pp. 284–293, Jan. 2012.
[27] Z. Lukic, N. Rahman, and A. Prodić, "Multi-bit Σ-Δ PWM digital controller IC for DC–DC converters operating at switching frequencies beyond 10 MHz," *IEEE Trans. Power Electron.*, vol. 22, no. 5, pp. 1693–1707, Sep. 2007.
[28] S. Saggini, P. Mattavelli, and G. Garcea, "A mixed-signal synchronous/asynchronous control for high-frequency dc–dc boost converters," *IEEE Trans. Ind. Electron.*, vol. 55, no. 5, pp. 2053–2060, May 2008.
[29] B. Patella, A. Prodić, A. Zirger, and D. Maksimović, "High-frequency digital PWM controller IC for DC/DC converters," *IEEE Trans. Power Electron.*, vol. 18, no. 1, pp. 438–446, Jan. 2003.
[30] Y. Halihal, Y. Bezdenezhnykh, I. Ozana, and M. M. Peretz, "Full FPGA-based design of a PWM/CPM controller with untegrated high-resolution fast ADC and DPWM peripherals," in *Proc. IEEE Workshop Control Model. Power Electron.*, Jun. 2014, pp. 1–5.
[31] V. Yousefzadeh and S. Choudhury, "Nonlinear digital PID controller for DC-DC converters," in *Proc. IEEE Appl. Power Electron. Conf. Expo.*, Feb. 2008, pp. 1704–1709.
[32] R. Venkataramanan, "*Sliding mode control of power converters*," Ph.D. dissertation, California Inst. Technol., Pasadena, CA, USA, May 1986.
[33] E. Santi, D. Li, A. Monti, and A. M. Stanković, "A geometric approach to large-signal stability of switching converters under sliding mode control and synergetic control," in *Proc. IEEE Power Electron. Spec. Conf.*, Jun. 2005, pp. 1389–1395.
[34] S. Tan, Y. Lai, and C. Tse, "Implementation of pulse-width-modulation based sliding mode controller for boost converters," *IEEE Power Electron. Lett.*, vol. 3, no. 4, pp. 130–135, Dec. 2005.
[35] S. Oucheriah and G. Liping, "PWM-based adaptive sliding-mode control for boost DC–DC converters," *IEEE Trans. Ind. Electron.*, vol. 60, no. 8, pp. 3291–3294, Aug. 2013.
[36] M. Ordonez, M. T. Iqbal, and J. E. Quaicoe, "Selection of a curved switching surface for buck converters," *IEEE Trans. Power Electron.*, vol. 21, no. 4, pp. 1148–1153, Jul. 2006.
[37] K. S. Leung and H. S. H. Chung, "Derivation of a second-order switching surface in the boundary control of buck converters," *IEEE Power Electron. Lett.*, vol. 2, no. 2, pp. 63–67, Jun. 2004.
[38] K. S. Leung and H. S. H. Chung, "A comparative study of the boundary control of buck converters using first- and second-order switching surfaces—Part I: Continuous conduction mode," in *Proc. IEEE Power Electron. Spec. Conf.*, Jun. 2005, pp. 2133–2139.
[39] K. S. Leung and H. S. H. Chung, "A comparative study of boundary control with first- and second-order switching surfaces for buck converters operating in DCM," *IEEE Trans. Power Electron.*, vol. 22, no. 4, pp. 1196–1209, Jul. 2007.
[40] W. W. Burns and T. G. Wilson, "A State trajectories used to observe and control DC-to-DC converter," *IEEE Trans. Aerosp. Electron. Syst.*, vol. 12, no. 6, pp. 706–717, Nov. 1976.
[41] W. W. Burns and T. G. Wilson, "Analytic derivation and evaluation of a state trajectory control law for dc-to-dc converters," in *Proc. Power Electron. Spec. Conf.*, 1977, pp. 70–85.
[42] B. C. Bao, G. H. Zhou, J. P. Xu, and Z. Liu, "Unified classification of operation-state regions for switching converters with ramp compensation," *IEEE Trans. Power Electron.*, vol. 26, no. 7, pp. 1968–1975, Jul. 2011.
[43] T. T. Song and H. S. H. Chung, "Boundary control of boost converters using state-energy plane," *IEEE Trans. Power Electron.*, vol. 23, no. 2, pp. 551–563, Mar. 2008.
[44] J. J. E. Slotine and W. Li, *Applied Nonlinear Control*. Englewood Cliffs, NJ, USA: Prentice-Hall, 1991.
[45] *DE2 Development and Education Board User Manual*, San Juse, CA, USA: Altera Corp., 2006.

Or Kirshenboim (S'15) was born in Haifa, Israel, in 1987. He received the B.Sc. and M.Sc. degrees in electrical and computer engineering from Ben-Gurion University of the Negev, Beer-Sheva, Israel, in 2013 and 2015, respectively, where he is currently working toward the Ph.D. degree in electrical and computer engineering.

His current research interests include digital, nonlinear and smart control methods for SMPS, hybrid voltage regulation solutions, pulsed power applications, and batteries balancing topologies.

Mor Mordechai Peretz (S'05–M'12) was born in Beer-Sheva, Israel, in 1979. He received the B.Tech. degree in electrical engineering from the Negev Academic College of Engineering, Beer-Sheva, in 2003, and the M.Sc. and Ph.D. degrees in electrical and computer engineering from Ben-Gurion University, Negev, Israel, in 2005 and 2010, respectively.

From 2010 to 2012, he was a Postdoctoral Fellow at the Laboratory for Power Management and Integrated SMPS, University of Toronto, Canada. In 2012, he joined the Department of Electrical and Computer Engineering, Ben-Gurion University, where he is currently the Director of the Center for Power Electronics and Mixed-Signal IC. His current research interests include digital and smart control methods for efficient energy processing, SMPS miniaturization, mixed-signal IC design of SMPS, modeling and computer aided design, applications of nonlinear magnetics, and renewable energy systems.

Dr. Peretz is currently as an Associate Editor of the IEEE TRANSACTIONS ON POWER ELECTRONICS and the IEEE JOURNAL OF EMERGING AND SELECTED TOPICS IN POWER ELECTRONICS.